Computational Mechanics 17 (1995) 49–61 © Springer-Verlag 1995

Continuum modelling of strong discontinuities in solid mechanics using damage models

J. Oliver

Abstract Numerical simulation of strong discontinuities by using standard stress-strain constitutive equations including strain-softening is addressed. The concept of strong discontinuity analysis is introduced and driven, as a matter of example, into a standard continuum damage model. Then, the relevant features that make the constitutive equation compatible with the appearance of strong discontinuities are extracted. Those features are used in the design of a specific finite element approach to the strong discontinuity problem which is placed in the framework of the assumed enhanced strain methods. Numerical simulations show that mesh size and mesh alignment dependencies, typical of some continuum approaches, can be removed.

1 Introduction

Strong discontinuities are understood here as jumps in the displacement field appearing in solids across discontinuity paths which are material surfaces. Strong discontinuities are of considerable interest in many engineering fields when the aim of the analysis is to approach limit situations close to intensive damage or collapse. Cracks in concrete or rocks, slip lines in soils and shear bands in metals (when observed from a macroscopic point of view) are examples of strong discontinuities appearing at a certain time (in general unknown) of the loading history and whose initiation and development along the solid are aimed to be modelled by the analysis.

The presently available methodologies for the numerical simulation of strong discontinuities could be classified in two families: discrete and continuum approaches.

Discrete approaches, see for instance Dvorkin, Cuitino and Gioia (1990), Lofti and Shing (1994), characterize in different ways the continuous and the discontinuous parts of the body. The discontinuity path is either stress free or the stress field is defined via specific constitutive equations relating the traction vector and the displacement jumps. The continuous part is modelled in a classical Continuum Mechanics environment. In general they need appropriate additional criteria for the determination of the direction of propagation of the discontinuity.

Continuum approaches intend to keep the whole analysis in a Continuum Mechanics framework. The concept of strain is defined everywhere in the solid and, consequently, stress-strain constitutive equations can be considered. Then the discontinuity is numerically modelled via two basic ingredients: a) an implicit (sometimes not recognized) regularization of the displacement jumps which are approximated by high displacement gradients (strain localization) in a band whose width is characterized by the so called characteristic length which is taken as a material property, Belytschko, Fish and Engelmann (1988), or as a numerical parameter, Oliver (1989), and b) special constitutive equations whose particular structure leads to the well posedness of the partial differential equations governing the problem and allowing the strain localization to appear. The smeared crack methods using (regularized) local constitutive equations exhibiting strain softening, Oliver, Cervera, Oller and Lubliner (1990), non local constitutive equations, Pijaudier Cabot and Bazant (1987), Cosserat continuum, gradient plasticity, De Borst, Mulhaus, Pamin and Sluys (1992), viscoplasticity, Needleman (1988), (or in general visco-regularized constitutive equations) are examples of approaches belonging to this family.

In this work, continuation of previous works on the subject, Simo, Oliver and Armero (1993), Oliver and Simo (1994), Simo and Oliver (1993), a somehow comprehensive approach is proposed. The concept of strong discontinuity analysis, whose aim is the identification of the key qualitative features that make standard stress-strain constitutive equations consistent with the appearance of strong discontinuities, is introduced. Special emphasis is placed in not involving any numerical method of simulation in this analysis. In particular, the analysis provides a set of consistent discrete (i.e., stress-displacement jump) constitutive equations at the discontinuity path, which link continuum approaches with the discrete ones. On the other hand a set of relevant points emerging from the strong discontinuity analysis can be directly used in the design of specific finite elements for capturing strong discontinuities, in such a way that many unsuitable features of classical continuum approaches (mesh-size and mesh-alignment dependencies, intrinsic limitations on the element size etc...) can be automatically removed.

An outline of the reminder of the paper is as follows. Section 2 introduces a suitable kinematic description of the discontinuous problem. Section 3 is devoted to the introduction of the strong discontinuity analysis which is applied to a family of continuum damage models in Sect. 4. In Sects. 5 and 6 the strong and weak forms of the resulting B.V.P are presented.

Communicated by S. N. Atluri, 18 August 1995

J. Oliver
E.T.S. d'Enginyers de Camins, Canals i Ports. Technical University of Catalonia, Gran Capità s/n. Mòdul C-1, 08034 Barcelona, Spain

To Prof. Juan C. Simo
"In memoriam"

A family of finite element approximations to the strong discontinuity problem is then introduced in Sect. 7. Finally, Sect. 8 is devoted to present some numerical simulations. Conclusions are drawn in Sect. 9.

2
Kinematics: Discontinuous displacement field

Let us consider the reference configuration Ω of a body exhibiting strong discontinuities along a discontinuity path $\mathscr{S}$ which is a material surface (fixed at the reference configuration) with a unit normal vector $\mathbf{n}$ (see Fig. 1a). For practical purposes we can assume that $\mathscr{S}$ splits the body into two parts Ω^+ and Ω^- in such a way that a Heaviside (step) function $H_{\mathscr{S}}(\mathbf{x})$ ($\mathbf{x}$ being the material coordinates of the particles, $H_{\mathscr{S}}(\mathbf{x}) = 1\,\forall\,\mathbf{x}\in\Omega^+$ and $H_{\mathscr{S}}(\mathbf{x}) = 0\,\forall\,\mathbf{x}\in\Omega^-$) can be defined on Ω. Let $\Gamma_u \subset \partial\Omega$ and $\Gamma_\sigma \subset \partial\Omega$ ($\Gamma_u \cup \Gamma_\sigma = \partial\Omega$, $\Gamma_u \cap \Gamma_\sigma = \varnothing$) be the boundaries of Ω subjected to the usual essential and natural boundary conditions, respectively. Let us consider, finally, an additional subdomain $\Omega^h \subset \Omega$ surrounding $\mathscr{S}$ ($\mathscr{S} \subset \Omega^h$ see Fig. 1b), defined by the two arbitrary boundaries ahead of ($\mathscr{S}_h^+$) and behind of ($\mathscr{S}_h^-$) the discontinuity surface, and splitted by $\mathscr{S}$ into the subdomains Ω_h^+ and Ω_h^-. It is assumed that the boundary Γ_u, where the essential boundary conditions are imposed, is outside Ω^h ($\Gamma_u \cap \Omega^h = \varnothing$). Then, we can define a continuous function $\varphi^h(\mathbf{x})$ which is completely arbitrary except for the following two conditions:

$$\varphi^h(\mathbf{x}) = 0 \quad \forall\mathbf{x}\in\Omega^-\setminus\Omega_h^-$$

$$\varphi^h(\mathbf{x}) = 1 \quad \forall\mathbf{x}\in\Omega^+\setminus\Omega_h^+ \tag{2.1}$$

Let us now consider the function $\mathscr{M}_{\mathscr{S}}^h(\mathbf{x})$ defined as:

$$\mathscr{M}_{\mathscr{S}}^h(\mathbf{x}) = H_{\mathscr{S}}(\mathbf{x}) - \varphi^h(\mathbf{x}) \tag{2.2}$$

It is straightforward to check that $\mathscr{M}_{\mathscr{S}}^h(\mathbf{x})$ (from now on termed the unit jump function) takes the value zero everywhere in Ω except in Ω_h (the support of $\mathscr{M}_{\mathscr{S}}^h$, see Fig. 2 for 1D cases) and exhibits a unit jump across $\mathscr{S}$. With these definitions in mind we can write a convenient expression for a displacement field

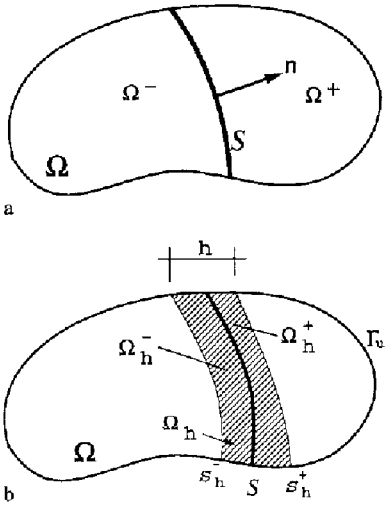

Fig. 1a–b. Definition of the discontinuity path

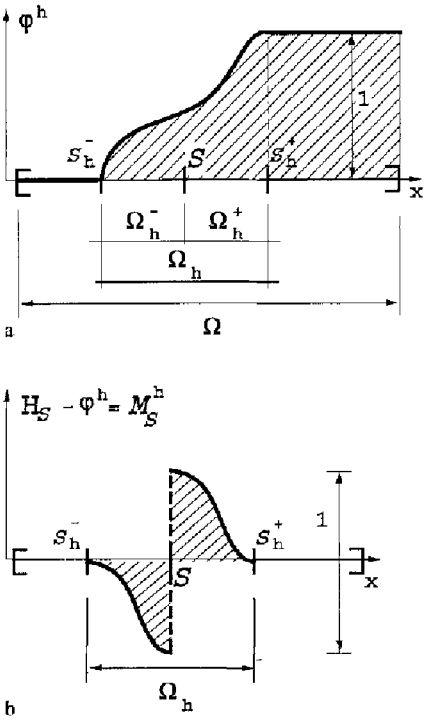

Fig. 2a–b. Construction of the unit jump function

$\mathbf{u}(\mathbf{x}, t)$ exhibiting a strong discontinuity in $\mathscr{S}$ as:

$$\mathbf{u}(\mathbf{x}, t) = \hat{\mathbf{u}}(\mathbf{x}, t) + \mathscr{M}_{\mathscr{S}}^h(\mathbf{x})[\![\mathbf{u}]\!](\mathbf{x}, t) \tag{2.3}$$

where $\hat{\mathbf{u}}(\mathbf{x}, t)$ is the regular (continuous) part of the displacement field and $[\![\mathbf{u}]\!](\mathbf{x}, t)$ is a continuous displacement jump function. From Eq. (2.3) a jump in $\mathbf{u}$ appears on $\mathscr{S}$ whose intensity is:

$$[\mathbf{u}^+(\mathbf{x}, t) - \mathbf{u}^-(\mathbf{x}, t)]_{\mathbf{x}\in\mathscr{S}} = [\![\mathbf{u}]\!](\mathbf{x}, t)|_{\mathbf{x}\in\mathscr{S}} = [\![\mathbf{u}]\!]_{\mathscr{S}} \tag{2.4}$$

where superscripts $(\cdot)^-$ $(\cdot)^-$ refer to values in Ω^+ and Ω^-, respectively. Observe that the kinematic description (2.3) allows the essential boundary conditions to be applied exclusively on the term $\hat{\mathbf{u}}(\mathbf{x}, t)$. This fact makes this kinematic description specially suitable for numerical simulations. As a matter of example in Fig. 3 the displacement field decomposition of Eq. (2.3) for 1D cases is depicted.

The corresponding strain field can be obtained by computing the symmetric part of the gradient of the displacement field (2.3), thus leading to:

$$\boldsymbol{\varepsilon} = (\nabla\mathbf{u})^S = \underbrace{\bar{\boldsymbol{\varepsilon}}}_{\text{bounded}} + \underbrace{\delta_{\mathscr{S}}([\![\mathbf{u}]\!]\otimes\mathbf{n})^S}_{\text{unbounded}} \tag{2.5}$$

where superscript $(\cdot)^S$ means the symmetric part of $(\cdot)$ and $\delta_{\mathscr{S}}$ is the surface (line in 2D cases) Dirac's delta-function along $\mathscr{S}$.

In Eq. (2.5) the term $\bar{\boldsymbol{\varepsilon}}$, is the regular part of the strain field collecting gradients of the continuous functions appearing in Eq. (2.3), thus exhibiting, at most, bounded discontinuities. The unbounded character of the term $\delta_{\mathscr{S}}([\![\mathbf{u}]\!]\otimes\mathbf{n})^S$ emerges from the gradient of the Heaviside function appearing in Eq. (2.2).

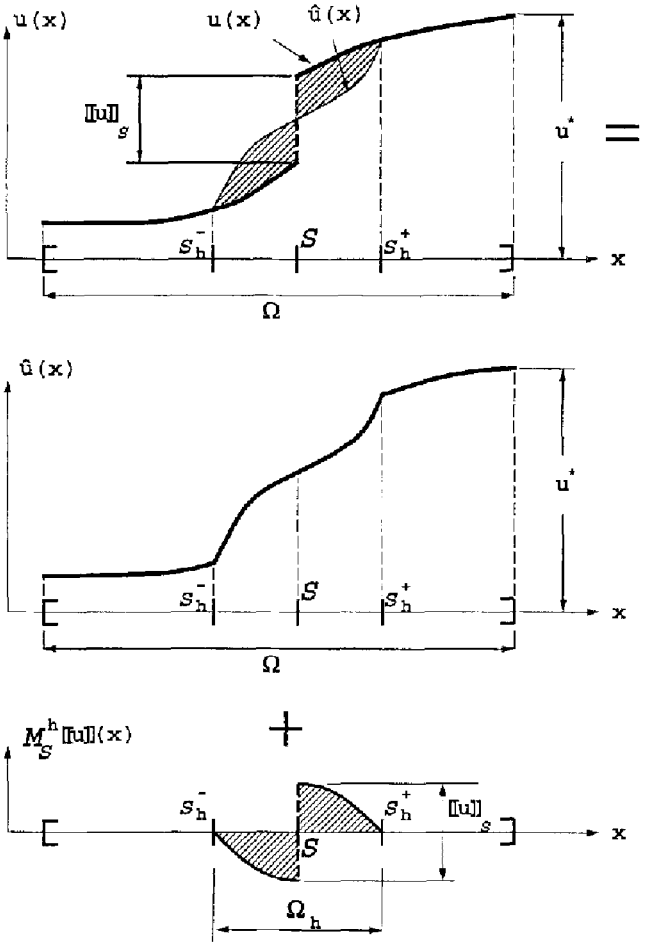

Fig. 3. Kinematics: decomposition of the displacement field

3
Strong discontinuity analysis

The concept of strong discontinuity analysis applies to any standard constitutive equation. The goal of the analysis is to extract the key qualitative features that make such a constitutive equation consistent with the appearance of strong discontinuities and, thus, with the unbounded strain field of Eq. (2.5). For this purpose the following set of requirements, on the stress field provided by the constitutive equation, are imposed:

I) The stress field is bounded everywhere in Ω.
II) The traction vector is continuous across S at any time of the analysis.
III) The normal $\mathbf{n}$ at any point of the discontinuity surface $\mathscr{S}$ is provided by the stress field at the initiation time (the time where the discontinuity initiates at the considered point).

Justification of condition I) comes from the non-physical sense of unbounded stresses (even at the discontinuity path $\mathscr{S}$, where the strains are unbounded according to Eq. (2.5)). Condition II) emerges from the equilibrium conditions across the discontinuity path or, more formally, from the balance laws (see Simo and Oliver (1994) for more details). Finally, condition III) establishes the material character of $\mathscr{S}$, thus precluding any evolution of $\mathbf{n}$ beyond the initiation time.

As a matter of example, in the next section the strong discontinuity analysis of a classical constitutive equation, belonging to the family of continuum damage models, is addressed.

4
Strong discontinuity analysis of damage models

4.1
An isotropic continuum damage model

Let us consider the family of constitutive equations defined by:

$$\boldsymbol{\sigma} = (1-d)\,\mathbf{C}:\boldsymbol{\varepsilon} \tag{4.1.1}$$

where $\mathbf{C}$ is the elastic constitutive tensor, $\boldsymbol{\sigma}$ the stress tensor and d the scalar damage variable ($0 \leqq d \leqq 1$). The value of the internal variable d is given by the corresponding damage condition and evolution laws. After some specialization, see Oliver, Cervera, Oller and Lubliner (1990), the damage variable evolution can be integrated in closed form at time t leading to:

$$d_t = G(r_t); \quad r_t = \max_{s\in(-\infty,t)} \{r_0, \tau_s^\varepsilon\} \tag{4.1.2}$$

In Eq. (4.1.2) τ^ε is an appropriate norm of the strains described below, r_0 is an initial threshold value and $G(\cdot)$ is a non-decreasing scalar function such that $G(r_0) = 0$, $G(\infty) \leqq 1$ and $G'(\mu) \geqq 0\ \forall\, \mu \in [r_0, \infty)$. The variable r_t describes, at time t, the size of the elastic domain in the strain space E_ε defined as:

$$E_{r_t} := \{\boldsymbol{\varepsilon} \mid \tau^\varepsilon \leqq r_t\}; \quad \tau^\varepsilon = \sqrt{\boldsymbol{\varepsilon}:\mathbf{C}:\boldsymbol{\varepsilon}} \tag{4.1.3}$$

Under such conditions it is straightforward to check that both d and r always increase along time ($\dot{d} \geqq 0$; $\dot{r} \geqq 0$). Unloading and elastic and neutral loading are characterized by $\dot{d} = 0$ whereas $\dot{d} > 0$ corresponds to inelastic loading. By specialization of the function $G(\cdot)$ and the norm τ^ε in Eqs. (4.1.3) different qualitative behaviours can be modelled, see Oliver, Cervera, Oller and Lubliner (1990). For the sake of simplicity it is considered here a linear strain hardening-softening law with symmetric tension-compression behaviour defined by:

$$d = G(r) = \begin{cases} 0 & r < r_0 = \sigma_u/\sqrt{E} \\ \dfrac{1}{1+\mathscr{H}}\left(1-\dfrac{r_0}{r}\right) & r_0 < r < r_{\max} = -\dfrac{1}{\mathscr{H}} r_0 \ (\text{for } \mathscr{H} < 0) \\ 1 & r_{\max} < r \end{cases} \tag{4.1.4}$$

In Eqs. (4.1.4) $\mathscr{H}$ plays the role of hardening-softening parameter, σ_u is the uniaxial peak stress and E is the Young modulus. The corresponding uniaxial stress-strain law is presented in Fig. 4. Observe, from Eqs. (4.1.1) and $(4.1.3)_2$, that a new norm τ^σ, in the stress space, could have been defined as:

$$\tau^\sigma = \sqrt{\boldsymbol{\sigma}:\mathbf{C}^{-1}:\boldsymbol{\sigma}} = (1-d)\sqrt{\boldsymbol{\varepsilon}:\mathbf{C}:\boldsymbol{\varepsilon}} = (1-d)\,\tau^\varepsilon \tag{4.1.5}$$

For the purposes of this analysis the norm τ^σ is more suitable than τ^ε, therefore in the following the model will be described in terms of τ^σ, keeping in mind that both norms are related through Eqs. (4.1.5). Finally, the dissipation for the considered model can be written in a suitable form as:

$$\mathscr{D} = \frac{1}{2}(\tau^\sigma)^2 \frac{\partial}{\partial t}\left(\frac{d}{1-d}\right) \geqq 0 \tag{4.1.6}$$

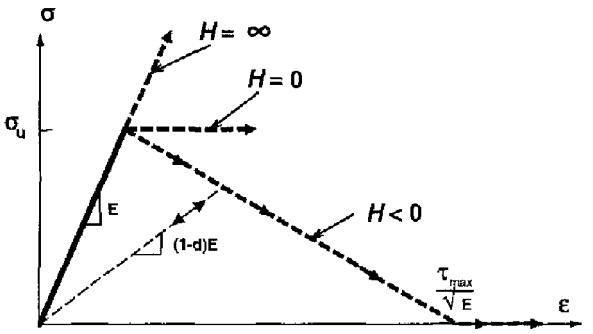

Fig. 4. Damage model: uniaxial stress-strain law

where the term $d/(1-d)$ can be expressed, under loading conditions, as:

$$\frac{d}{1-d}=\frac{1}{\mathscr{H}}g;\quad g(\boldsymbol{\sigma})=1-\frac{r_0}{\tau^e(\boldsymbol{\sigma})} \tag{4.1.7}$$

Remark 4.1.1 Observe from Eqs. (4.1.5) and (4.1.7) that if the stresses are bounded (and different from zero) so is g. Also observe that negative values of the hardening-softening parameter ($\mathscr{H}<0 \Rightarrow$ strain softening) keep the stresses bounded for any value (even unbounded) of the strain field (see Fig. 4 for 1D cases). This facts will be conveniently exploited in next sections.

4.2 Condition I): Stress boundedness

The constitutive equation (4.1.1) can be conveniently rephrased as:

$$\left(1+\frac{d}{1-d}\right)\boldsymbol{\sigma}=\mathbf{C}:\boldsymbol{\varepsilon} \tag{4.2.1}$$

and, by substitution of the strain field (2.5) into Eq. (4.2.1), we arrive to:

$$\underbrace{\boldsymbol{\sigma}}_{\text{bounded}}+\frac{d}{1-d}\boldsymbol{\sigma}=\underbrace{\mathbf{C}:\bar{\boldsymbol{\varepsilon}}}_{\text{bounded}}+\underbrace{\delta_{\mathscr{S}}\mathbf{C}:(\bar{\llbracket\mathbf{u}\rrbracket}_{\mathscr{S}}\otimes\mathbf{n})^{\delta}}_{\text{unbounded}} \tag{4.2.2}$$

Inspection of Eq. (4.2.2) reveals that if we impose the stress field to be bounded, then the first term of the left-hand side is bounded and so is the first term of the right-hand side due to the bounded nature of $\bar{\boldsymbol{\varepsilon}}$ (see Eq. (2.5)). Moreover, as we are looking for discontinuous solutions of the problem, then $\llbracket\mathbf{u}\rrbracket_{\mathscr{S}}\neq 0$ and, thus, the last term of Eq. (4.2.2) is unbounded. Finally, in order to make the whole equation have mathematical sense, this unbounded term has to be cancelled by some additional unbounded (including a delta-function term in Eq. (4.2.2) the only available candidate being $d/(1-d)$. Since inspection of this term in Eq. (4.1.7) reveals that g is bounded[1] (see Remark 4.1.1) the only possibility is:

$$\frac{1}{\mathscr{H}}=\underbrace{\delta_{\mathscr{S}}\frac{1}{\bar{\mathscr{H}}}}_{\text{unbounded}}+\underbrace{\frac{1}{\mathscr{H}^*}}_{\text{regular}} \tag{4.2.3}$$

[1] The case $\boldsymbol{\sigma}=\mathbf{0}$ also applies here since $g\boldsymbol{\sigma}$ can be shown to be bounded in this case

For the sake of simplicity we will restrict in the following to the particular case $1/\mathscr{H}^*=0$ (the analysis could be continued for the general case but no relevant insight in the problem is gained), so that:

$$\frac{1}{\mathscr{H}}=\delta_{\mathscr{S}}\frac{1}{\bar{\mathscr{H}}} \tag{4.2.4}$$

Equation (4.2.4) states a crucial consequence of the stress boundedness requirement, that is: the distributional character of the softening parameter $\mathscr{H}$ whose inverse has the structure of a delta-function with intensity $1/\bar{\mathscr{H}}$. Parameter $\bar{\mathscr{H}}$ will be termed from now on the intrinsic softening parameter.

By substitution of Eq. (4.2.4) into Eq. (4.1.7) and then into Eq. (4.2.2) we arrive to:

$$\underbrace{[\boldsymbol{\sigma}-\mathbf{C}:\bar{\boldsymbol{\varepsilon}}]}_{=0\text{ on }\Omega\backslash\mathscr{S}}=\delta_{\mathscr{S}}\underbrace{\left[\mathbf{C}:(\llbracket\mathbf{u}\rrbracket\otimes\mathbf{n})^{\delta}-\frac{1}{\bar{\mathscr{H}}}g\boldsymbol{\sigma}\right]}_{=0\text{ on }\mathscr{S}} \tag{4.2.5}$$

In order to Eq. (4.2.5) have mathematical sense the underbraced terms of the left and the right hand sides have to cancel in the continuous ($\Omega\backslash\mathscr{S}$) and discontinuous ($\mathscr{S}$) parts of Ω, respectively. Thus, the corresponding stress fields emerge from Eq. (4.2.5) as:

$$\boldsymbol{\sigma}_{\Omega\backslash\mathscr{S}}=\mathbf{C}:\bar{\boldsymbol{\varepsilon}} \tag{4.2.6}$$

$$\boldsymbol{\sigma}_{\mathscr{S}}=\frac{\bar{\mathscr{H}}}{g(\boldsymbol{\sigma}_{\mathscr{S}})}\mathbf{C}:(\llbracket\mathbf{u}\rrbracket_{\mathscr{S}}\otimes\mathbf{n})^{\delta} \tag{4.2.7}$$

Remark 4.2.1 Equation (4.2.6) states the elastic behaviour in the continuous part of the body ($\Omega\backslash\mathscr{S}$) in terms of the corresponding strain field $\bar{\boldsymbol{\varepsilon}}$. A non linear behaviour could have been considered by using the whole Eq. (4.2.3) instead of the simplified Eq. (4.2.4).

Remark 4.2.2 Equation (4.2.7) provides a discrete non-linear stress-jump constitutive equation at the interface $\mathscr{S}$ which allows the determination of the complete stress tensor, $\boldsymbol{\sigma}_{\mathscr{S}}=\boldsymbol{\sigma}_{\mathscr{S}}(\llbracket\mathbf{u}\rrbracket_{\mathscr{S}},\mathbf{n})$ in terms of the jump $\llbracket\mathbf{u}\rrbracket_{\mathscr{S}}$ and the normal $\mathbf{n}$. So, unlike what is usual in constitutive equations for discontinuity interfaces, not only the traction vector is involved. Moreover, this discrete constitutive equation is consistent (emerges naturally from the stress boundedness requirement) with the original continuous constitutive equation described in Sect. 4.1.

Remark 4.2.3 Observe that the arguments employed to obtain Eq. (4.2.7) can be reversed in the following sense: if a) the distributional character of the hardening-softening parameter, Eq. (4.2.4), is enforced (consequently the elastic behaviour defined by Eq. (4.2.6) is imposed in $\Omega\backslash\mathscr{S}$) and b) strain-softening is considered for the constitutive behaviour at $\mathscr{S}$ ($\bar{\mathscr{H}}<0$), then the stresses are bounded both in $\Omega\backslash\mathscr{S}$ (since $\bar{\boldsymbol{\varepsilon}}$ is bounded in Eq. (4.2.6)) and in $\mathscr{S}$ (see Remark 4.1.1). Therefore, Eq. (4.2.7) automatically fulfills from the imposition of the standard constitutive Eq. (4.1.1) through consistency of Eq. (4.2.5). This argument reveals crucial to avoid the explicit imposition of Eqs. (4.2.7), which are specific (and

sometimes difficult to derive) of the considered constitutive equation, and it will be exploited in the numerical simulation of the problem.

4.3
Condition II): Traction vector continuity

Traction vector continuity across $\mathscr{S}$ reads[2]:

$$\boldsymbol{\sigma}_{\Omega\setminus\mathscr{S}}|_{\mathbf{x}\in\mathscr{S}}\cdot\mathbf{n}=\boldsymbol{\sigma}_{\mathscr{S}}\cdot\mathbf{n} \tag{4.3.1}$$

and from Eqs. (4.2.6) ad (4.2.7):

$$\mathbf{n}\cdot\mathbf{C}:\bar{\boldsymbol{\varepsilon}}_{\mathscr{S}}=\frac{\bar{\mathscr{H}}}{g_{\mathscr{S}}}\mathbf{n}\cdot\mathbf{C}:(\llbracket\mathbf{u}\rrbracket_{\mathscr{S}}\otimes\mathbf{n})^{S}=\frac{\bar{\mathscr{H}}}{g_{\mathscr{S}}}\mathbf{n}\cdot\mathbf{C}\cdot\mathbf{n}\cdot\llbracket\mathbf{u}\rrbracket_{\mathscr{S}} \tag{4.3.2}$$

$$\llbracket\mathbf{u}\rrbracket_{\mathscr{S}}=\frac{g(\boldsymbol{\sigma}_{\mathscr{S}}(\llbracket\mathbf{u}\rrbracket_{\mathscr{S}},\mathbf{n}))}{\bar{\mathscr{H}}}\mathbf{Q}^{e-1}\cdot\mathbf{n}\cdot\mathbf{C}:\bar{\boldsymbol{\varepsilon}}_{\mathscr{S}}$$

$$\mathbf{Q}^{e}=\mathbf{n}\cdot\mathbf{C}\cdot\mathbf{n} \tag{4.3.3}$$

where $\mathbf{Q}^e$ is the so called elastic acoustic tensor, Willam and Sobh (1987).

Remark 4.3.1 Equation (4.3.3), in view of Eq. (4.2.7), provides the jump $\llbracket\mathbf{u}\rrbracket_{\mathscr{S}}$ in terms of the regular part of the strains $\bar{\boldsymbol{\varepsilon}}_{\mathscr{S}}$ and the normal $\mathbf{n}$. Again, it is emphasized that Eqs. (4.3.3), dependent on the considered type of constitutive equation, need not be explicitly derived for simulation purposes. The relevant fact, exploited below, is that the traction vector continuity requirement of Eq. (4.3.1) provides the set of equations which determines the jump.

4.4
Condition III): Identification of the normal

Let us consider a material point P belonging to the discontinuity surface $\mathscr{S}$ and let $t_0<t$ be the time at which the discontinuity initiates at P (the initiation time) characterized by:

$$\llbracket\mathbf{u}\rrbracket(\mathbf{x}_P,t_0)=\llbracket\mathbf{u}\rrbracket^0_{\mathscr{S}}=0$$

$$\llbracket\dot{\mathbf{u}}\rrbracket(\mathbf{x}_P,t_0)=\llbracket\dot{\mathbf{u}}\rrbracket^0_{\mathscr{S}}\neq 0 \tag{4.4.1}$$

Equation (4.2.7) can be rewritten as:

$$g_{\mathscr{S}}\boldsymbol{\sigma}_{\mathscr{S}}=\bar{\mathscr{H}}\mathbf{C}:(\llbracket\mathbf{u}\rrbracket_{\mathscr{S}}\otimes\mathbf{n})^{S} \tag{4.4.2}$$

and taking time derivatives in Eq. (4.4.2) we get:

$$\dot{g}_{\mathscr{S}}\boldsymbol{\sigma}_{\mathscr{S}}+g_{\mathscr{S}}\dot{\boldsymbol{\sigma}}_{\mathscr{S}}=\bar{\mathscr{H}}\mathbf{C}:(\llbracket\dot{\mathbf{u}}\rrbracket_{\mathscr{S}}\otimes\mathbf{n})^{S} \tag{4.4.3}$$

where the character of material surface of $\mathscr{S}$ has been considered ($\dot{\mathbf{n}}=\mathbf{0}$). Equation (4.4.3) holds at any time and, in particular, at the initiation time t_0, where according to Eq. (4.4.1)$_1$ $\llbracket\mathbf{u}\rrbracket^0_{\mathscr{S}}=0$, so that from Eq. (4.4.2) $g^0_{\mathscr{S}}=0$ and Eq. (4.4.3) leads to:

$$\dot{g}^0_{\mathscr{S}}\boldsymbol{\sigma}^0_{\mathscr{S}}=\bar{\mathscr{H}}\mathbf{C}:(\llbracket\dot{\mathbf{u}}\rrbracket^0_{\mathscr{S}}\otimes\mathbf{n})^{S} \tag{4.4.4}$$

On the other hand since at the initiation time $\llbracket\mathbf{u}\rrbracket^0_{\mathscr{S}}=0$ and $g^0_{\mathscr{S}}=0$ then $\boldsymbol{\varepsilon}^0_{\mathscr{S}}=\bar{\boldsymbol{\varepsilon}}^0_{\mathscr{S}}$ and $d^0=0$ (see Eqs. (2.5) and (4.1.7), respectively) and finally one can write from Eq. (4.1.1):

$$\boldsymbol{\sigma}^0_{\mathscr{S}}=\mathbf{C}:\bar{\boldsymbol{\varepsilon}}^0_{\mathscr{S}} \tag{4.4.5}$$

Substituting Eq. (4.4.5) into Eq. (4.4.4) we arrive to:

$$\mathbf{C}:(\llbracket\dot{\mathbf{u}}\rrbracket^0_{\mathscr{S}}\otimes\mathbf{n})^{S}=\frac{\dot{g}^0_{\mathscr{S}}}{\bar{\mathscr{H}}}\boldsymbol{\sigma}^0_{\mathscr{S}}=\frac{\dot{g}^0_{\mathscr{S}}}{\bar{\mathscr{H}}}\mathbf{C}:\bar{\boldsymbol{\varepsilon}}^0_{\mathscr{S}} \tag{4.4.6}$$

and premultiplying both sides of Eq. (4.4.6) times $\mathbf{C}^{-1}$:

$$(\llbracket\dot{\mathbf{u}}\rrbracket^0_{\mathscr{S}}\otimes\mathbf{n})^{S}=\frac{\dot{g}^0_{\mathscr{S}}}{\bar{\mathscr{H}}}\bar{\boldsymbol{\varepsilon}}^0_{\mathscr{S}} \tag{4.4.7}$$

Equation (4.4.7) provides a set of equations for the determination of both $\llbracket\dot{\mathbf{u}}\rrbracket^0_{\mathscr{S}}$ and $\mathbf{n}$. In particular the normal $\mathbf{n}$ can be determined by taking advantage of the structure of the left-hand-side of Eq. (4.4.7). In fact, pre and post multiplying both sides of the equation by *any* vector $\mathbf{t}$ orthogonal to $\mathbf{n}$, the left-hand-side of Eq. (4.4.7) cancels, therefore:

$$\mathbf{t}\cdot(\llbracket\dot{\mathbf{u}}\rrbracket^0_{\mathscr{S}}\otimes\mathbf{n})^{S}\cdot\mathbf{t}=0=\frac{\dot{g}^0_{\mathscr{S}}}{\bar{\mathscr{H}}}\mathbf{t}\cdot\bar{\boldsymbol{\varepsilon}}^0_{\mathscr{S}}\cdot\mathbf{t} \tag{4.4.8}$$

so that:

$$\mathbf{t}\cdot\bar{\boldsymbol{\varepsilon}}^0_{\mathscr{S}}\cdot\mathbf{t}=0\quad\forall\,\mathbf{t}|\,\mathbf{t}\cdot\mathbf{n}=0 \tag{4.4.9}$$

Remark 4.4.1 Equation (4.4.9) is sufficient for the determination of the normal $\mathbf{n}$ at any point of $\mathscr{S}$ in terms of the regular (bounded) part of the strains $\bar{\boldsymbol{\varepsilon}}^0_{\mathscr{S}}$ (or in terms of the stresses through Eq. (4.4.5)) at the initiation time. In particular, for 2D cases, when the normal and tangent vectors can be defined by an inclination angle θ with respect to an orthogonal basis $\hat{\mathbf{e}}_1$ and $\hat{\mathbf{e}}_2$ as:

$$\begin{aligned}\mathbf{n}&=\cos\theta\hat{\mathbf{e}}_1+\sin\theta\hat{\mathbf{e}}_2\\ \mathbf{t}&=-\sin\theta\hat{\mathbf{e}}_1+\cos\theta\hat{\mathbf{e}}_2\end{aligned} \tag{4.4.10}$$

substitution of Eq. (4.4.10) into Eq. (4.4.9) leads, after some straightforward computations, to the following closed form solution for θ:

$$\theta=\operatorname{atan}\left[\frac{\bar{\varepsilon}^0_{12}\pm\sqrt{(\bar{\varepsilon}^0_{12})^2-\bar{\varepsilon}^0_{11}\bar{\varepsilon}^0_{22}}}{\bar{\varepsilon}^0_{11}}\right]_{\mathscr{S}} \tag{4.4.11}$$

providing two, in general different, possible solutions for the normal.

4.5
Dissipation: The fracture energy

Let us now consider the dissipated energy along the deformation process. From Eqs. (4.1.6) and (4.1.7) the dissipation can be written as:

$$\mathscr{D}=\frac{1}{2\mathscr{H}}(\tau^{\sigma})^2\dot{g}=\frac{r_0}{2\mathscr{H}}\dot{\tau}^{\sigma} \tag{4.5.1}$$

and substituting Eq. (4.2.4) into (4.5.1) we arrive to:

$$\mathscr{D}=\delta_{\mathscr{S}}\frac{r_0}{2\bar{\mathscr{H}}}\dot{\tau}^{\sigma}_{\mathscr{S}} \tag{4.5.2}$$

[2] No distinction is made between the traction vector at the positive (Ω^+) or negative (Ω^-) neighborhoods of $\mathscr{S}$, which are assumed to be the same from the balance laws Simo and Oliver (1994).

Let us imagine the deformation process, leading to the formation of the strong discontinuity at a certain material point of $\mathscr{S}$, as follows: the process starts at time $t=0$ with $(\tau^\sigma, d)=(0,0)$, then the stresses increase elastically (with no dissipation) until the initial threshold value r_0 is reached at time t_0, when $(\tau^\sigma, d)=(r_0, 0)$, finally a monotonic loading process ($\dot{d}\neq 0$) is driven up to the total stress relaxation at time t_1 with $(\tau^\sigma, d)=(0,1)$. The local energy release, u, along the process can be computed from Eq. (4.5.2) as:

$$u(\mathbf{x})=\int_{t_0}^{t_1}\mathscr{D}\,dt=\delta_{\mathscr{S}}\frac{r_0}{2\bar{\mathscr{H}}}\int_{\tau_0^\sigma}^{\tau_1^\sigma}d(\tau^\sigma)=-\delta_S\frac{r_0^2}{2\bar{\mathscr{H}}} \tag{4.5.3}$$

and the spent energy in the entire body can be obtained as:

$$\mathscr{U}=\int_\Omega u\,d\Omega=\int_\Omega-\delta_{\mathscr{S}}\frac{r_0^2}{2\bar{\mathscr{H}}}\,d\Omega=\int_{\mathscr{S}}-\frac{r_0^2}{2\bar{\mathscr{H}}}\,d\Gamma \tag{4.5.4}$$

The kernel of the last integral in Eq. (4.5.4) corresponds to the dissipated energy per unit surface at the discontinuity path $\mathscr{S}$, which can be immediately identified as the so called fracture energy G_f, that is:

$$G_f=-\frac{r_0^2}{2\bar{\mathscr{H}}} \tag{4.5.5}$$

Finally, considering Eq. $(4.1.4)_1$, Eq. (4.5.5) can be solved for $\bar{\mathscr{H}}$ as:

$$\bar{\mathscr{H}}=-\frac{r_0^2}{2G_f}=-\frac{\sigma_u^2}{2G_fE} \tag{4.5.6}$$

which states that the intrinic softening parameter $\bar{\mathscr{H}}$ is a material property related to the fracture energy G_f, Young modulus E and uniaxial peak stress σ_u. The negative value of $\bar{\mathscr{H}}$ is also stated there.

5
Field equations

The field equations governing the boundary value problem can be written as:

$$\nabla\cdot\boldsymbol{\sigma}+\mathbf{f}=\mathbf{0} \quad \text{in } \Omega\backslash\mathscr{S} \tag{5.1}$$

$$\mathbf{u}=\mathbf{u}^* \quad \text{in } \Gamma_u \tag{5.2}$$

$$\boldsymbol{\sigma}\cdot\boldsymbol{\nu}=\mathbf{t}^* \quad \text{in } \Gamma_\sigma \tag{5.3}$$

$$\boldsymbol{\sigma}^+\cdot\mathbf{n}=\boldsymbol{\sigma}^-\cdot\mathbf{n} \quad \text{in } \mathscr{S} \tag{5.4}$$

$$\boldsymbol{\sigma}_{\mathscr{S}}\cdot\mathbf{n}=\boldsymbol{\sigma}^+\cdot\mathbf{n}\,(=\boldsymbol{\sigma}^-\cdot\mathbf{n}) \quad \text{in } \mathscr{S} \tag{5.5}$$

Equation (5.1), where f corresponds to the body forces, is the classical equilibrium equation for the quasistatic problem. Equations (5.2) and (5.3) state the essential and natural boundary conditions, respectively ($\mathbf{u}^*$ and $\mathbf{t}^*$ are the prescribed displacement and traction vectors, respectively, and $\boldsymbol{\nu}$ is the outward normal to the external boundary $\partial\Omega$). Equations (5.4) and (5.5) state the continuity of the traction vector across the discontinuity surface $\mathscr{S}$. In particular, Eq. (5.4), where $\boldsymbol{\sigma}^+$ and $\boldsymbol{\sigma}^-$ stand for the stress fields on Ω^+ and Ω^-, respectively, involves the traction vectors ($\boldsymbol{\sigma}^+\cdot\mathbf{n}$ and $\boldsymbol{\sigma}^-\cdot\mathbf{n}$) at both sides of $\mathscr{S}$ whereas, in Eq. (5.5) the traction vector in the discontinuity surface ($\boldsymbol{\sigma}_{\mathscr{S}}\cdot\mathbf{n}$) is also involved. Equations (5.1) to (5.3) are the field equations for classical (continuous) problems, Eq. (5.4) is included when considering weak discontinuities whereas Eq. (5.5) is specific of problems exhibiting strong discontinuities.

6
Weak formulation

Let us consider the virtual work principle stating:

$$\int_\Omega\boldsymbol{\sigma}:\nabla\hat{\boldsymbol{\eta}}\,d\Omega=\int_\Omega\mathbf{f}\cdot\hat{\boldsymbol{\eta}}\,d\Omega+\int_{\Gamma_\sigma}\mathbf{t}^*\cdot\hat{\boldsymbol{\eta}}\,d\Gamma \tag{6.1}$$

for all the admissible test functions $\hat{\boldsymbol{\eta}}\in\hat{\mathscr{V}}$, where $\hat{\mathscr{V}}$ is the space of the continuous kinematically admissible variations defined by:

$$\hat{\mathscr{V}}:=\{\hat{\boldsymbol{\eta}}\in\mathscr{C}^0\ \hat{\boldsymbol{\eta}}|_{\Gamma_u}=\mathbf{0}\} \tag{6.2}$$

Integration by parts of Eq. (6.1), and standard arguments, lead to the following Euler equations for the variational problem:

$$\begin{aligned}&\nabla\cdot\boldsymbol{\sigma}+\mathbf{f}=\mathbf{0} && \text{in } \Omega\backslash\mathscr{S}\\ &\boldsymbol{\sigma}\cdot\boldsymbol{\nu}=\mathbf{t}^* && \text{in } \Gamma_\sigma\\ &\boldsymbol{\sigma}^+\cdot\mathbf{n}=\boldsymbol{\sigma}^-\cdot\mathbf{n} && \text{in } \mathscr{S}\end{aligned} \tag{6.3}$$

Comparing Eq. (6.3) with the field equations we realize that Eqs. (5.1), (5.3) and (5.4) are satisfied in weak form by application of the variational principle (6.1). Therefore, besides the standard essential boundary conditions (5.2), only the traction vector continuity condition (5.5) has to be locally enforced at the discontinuity surface $\mathscr{S}$.

7
Finite element approximation

For the sake of simplicity we will restrict in the following to 2D cases, although the extension to 3D cases follows quite naturally.

Let us consider a finite element discretization of Ω based on linear triangular elements as shown in Fig. 5. Let us also consider the band of finite elements crossed by $\mathscr{S}$, defining the subdomain Ω_h, and then the lines $\mathscr{S}_h^+$ and $\mathscr{S}_h^-$ which are constituted by the sides of the elements belonging to Ω_h and placed ahead of and behind of $\mathscr{S}$, respectively. Each element e of this band has one side (defined by the nodes i_e and j_e, see Fig. 5b) belonging to $\mathscr{S}_h^-$ (or to $\mathscr{S}_h^+$) and one node k_e belonging to $\mathscr{S}_h^+$ (or to $\mathscr{S}_h^-$). Let $\mathscr{S}_e$ be the straight segment of length l_e approaching $\mathscr{S}$ inside the element and $\mathbf{n}_e$ the normal to $\mathscr{S}_e$ (assumed to point to k_e).

7.1
Displacement and strain fields

Motivated by the kinematic description (2.3) we assume the following approximation to the displacement field:

$$\mathbf{u}^h(\mathbf{x},t)=\underbrace{\mathbf{N}(\mathbf{x})\cdot\mathbf{a}(t)}_{\hat{\mathbf{u}}^h(\mathbf{x},t)}+\sum_{e=1}^{n_{el}}\mathscr{M}^h_{\mathscr{S}_e}(\mathbf{x})\underbrace{\boldsymbol{\alpha}_e(t)}_{[\mathbf{u}]^h(t)} \tag{7.1.1}$$

$$\mathscr{M}^h_{\mathscr{S}_e}(\mathbf{x})=H_{\mathscr{S}_e}(\mathbf{x})-N_{k_e}(\mathbf{x}) \tag{7.1.2}$$

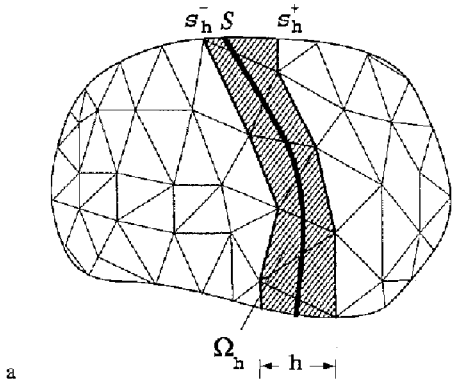

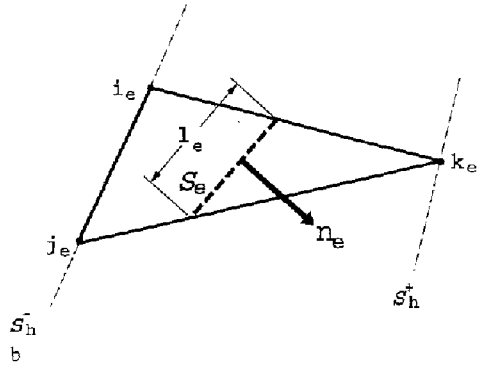

Fig. 5a–b. Finite element approximation to the strong discontinuity problem

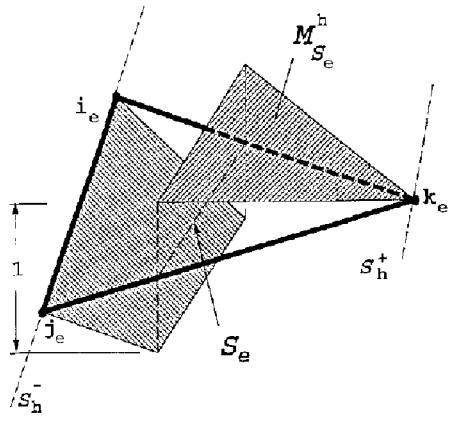

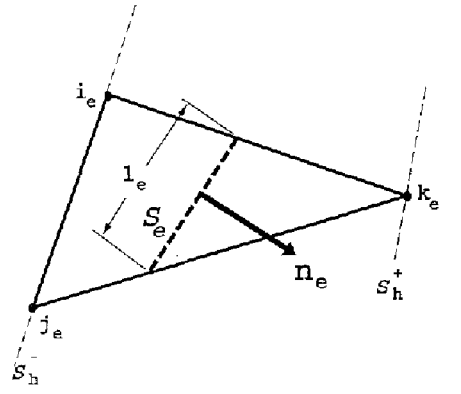

Fig. 6a–b. Finite element approximation of the unit jump function

where $\mathbf{N}(\mathbf{x})$ is the standard shape function matrix, Zienkiewicz and Taylor (1989), $\mathbf{a}(t)$ is the nodal displacements vector, $H_{\mathscr{S}_e}(\mathbf{x})$ is the Heaviside function restricted to the domain Ω_e, $N_{k_e}(\mathbf{x})$ is the standard linear shape function corresponding to the node k_e and n_{el} is the number of elements of the finite element mesh. Function $\mathscr{M}^h_{\mathscr{S}_e}(\mathbf{x})$ defined in Eq. (7.1.2) is depicted in Fig. 6 Therefore, in Eqs. (7.1.1) the term $\mathbf{N}(\mathbf{x})\cdot\mathbf{a}(t)$ matches the regular (smooth) part $\hat{\mathbf{u}}(\mathbf{x}, t)$ of the displacement field, and the essential boundary conditions have to be imposed on the corresponding nodal values $\mathbf{a}(t)$ as is usual in standard finite element approximations. The jump function $[\![\mathbf{u}]\!](\mathbf{x}, t)$ is approximated in a piece-wise constant manner (over the elements) and $\boldsymbol{\alpha}_e(t)$ plays the role of the displacement jump corresponding to the element e. From Eq. (7.1.1) the strain field is computed as the local (at elemental level) gradient of the displacement field:

$$\boldsymbol{\varepsilon}^h(\mathbf{x}, t) = \underbrace{(\nabla\hat{\mathbf{u}}^h)^S}_{\text{regular } \hat{\boldsymbol{\varepsilon}}^h} + \underbrace{\sum_{e=1}^{n_{el}} (\nabla\mathscr{M}^h_{\mathscr{S}_e}\otimes\boldsymbol{\alpha}_e)^S}_{\text{enhanced } \tilde{\boldsymbol{\varepsilon}}^h} \tag{7.1.3}$$

where, from Eq. (7.1.2):

$$\nabla\mathscr{M}^h_{\mathscr{S}_e} = \delta_{\mathscr{S}_e}\mathbf{n}_e - \nabla N_{k_e} \quad \forall\mathbf{x}\in\Omega_e \tag{7.1.4}$$

and $\delta_{\mathscr{S}_e}$ is the Dirac's delta-function, placed on $\mathscr{S}_e$ and restricted to the domain Ω_e.

Remark 7.1 The displacement and strain fields defined in Eqs. (7.1.1) and (7.1.3) inscribe the proposed approach in the method of the incompatible modes, see Simo and Rifai (1990), and the term $\mathscr{M}^h_{\mathscr{S}_e}\boldsymbol{\alpha}_e$ in Eq. (7.1.1), can be then interpreted as the incompatible mode corresponding to the element e.

It is expected that the modal amplitudes $\boldsymbol{\alpha}_e$ are zero for all the elements except for those defining the discontinuity path Ω_h (see Fig. 5a). The term $(\nabla\mathscr{M}^h_{\mathscr{S}_e}\otimes\boldsymbol{\alpha}_e)^S$ can be understood as the enhanced strain $\tilde{\boldsymbol{\varepsilon}}^h_e$, piece-wisely defined on each element e, enriching the regular strain field $\hat{\boldsymbol{\varepsilon}} = (\nabla\hat{\mathbf{u}}^h)^S$.

When dealing, as is usual for coding purposes, with the strain ($\boldsymbol{\varepsilon} = \{\varepsilon_{xx}, \varepsilon_{yy}, \gamma_{xy}\}$) and the stress ($\boldsymbol{\sigma} = \{\sigma_{xx}, \sigma_{yy}, \tau_{xy}\}$) vectors instead of the symmetric strain and stress tensors, the strain field (7.1.3) can be reformulated from Eqs. (7.1.1) and (7.1.4) in a cartesian (x, y) system of coordinates as:

$$\boldsymbol{\varepsilon}^h = \hat{\boldsymbol{\varepsilon}}^h + \sum_{e=1}^{n_{el}} \tilde{\boldsymbol{\varepsilon}}^h_e; \quad \hat{\boldsymbol{\varepsilon}}^h = \mathbf{B}\cdot\mathbf{a}; \quad \tilde{\boldsymbol{\varepsilon}}^h_e = \mathbf{G}_e\cdot\boldsymbol{\alpha}_e \tag{7.1.5}$$

$$\mathbf{G}_e(\mathbf{x}) = \begin{bmatrix} \delta_{\mathscr{S}_e}n_x - \dfrac{\partial N_{k_e}}{\partial x} & 0 \\ 0 & \delta_{\mathscr{S}_e}n_y - \dfrac{\partial N_{k_e}}{\partial y} \\ \delta_{\mathscr{S}_e}n_y - \dfrac{\partial N_{k_e}}{\partial y} & \delta_{\mathscr{S}_e}n_x - \dfrac{\partial N_{k_e}}{\partial x} \end{bmatrix} \quad \forall\mathbf{x}\in\Omega_e \tag{7.1.6}$$

where $\mathbf{B}$ is the standard deformation matrix, Zienkiewicz and Taylor (1989), and n_x and n_y are the components of $\mathbf{n}_e$ ($\mathbf{n}_e = \{n_x, n_y\}$).

7.2 Discretized set of equations

We now consider the finite element approximation to the weighting space $\hat{\mathscr{V}}$ of Eq. (6.2) given by:

$$\hat{\mathscr{V}}^h := \{\hat{\boldsymbol{\eta}}^h \mid \hat{\boldsymbol{\eta}}^h = \mathbf{N}\cdot\mathbf{a} \quad \hat{\boldsymbol{\eta}}^h|_{\Gamma_u} = \mathbf{0}\} \tag{7.2.1}$$

Substitution of Eq. (7.2.1) into Eq. (6.1) leads, through standard arguments, to the following set of equations:

$$\int_{\Omega} \mathbf{B}^T : \boldsymbol{\sigma}^h \, d\Omega = \underbrace{\int_{\Omega} \mathbf{N}^T \cdot \mathbf{f} \, d\Omega + \int_{\Gamma_\sigma} \mathbf{N}^T \cdot \mathbf{t}^* \, d\Gamma}_{\mathbf{f}_{ext}} \tag{7.2.2}$$

where superscript $(\cdot)^T$ means transposition of $(\cdot)$. Equations (7.2.2) are the discrete counterpart of the weak form (6.1).

As stated in section 6 the set of Eq. (7.2.2) would have to be complemented by the local enforcement of the traction vector continuity condition (5.5). Let us consider, instead, the following set of equations:

$$\int_{\Omega_e} \mathbf{G}_e^{*T} \cdot \boldsymbol{\sigma}^h \, d\Omega_e = 0 \quad e = 1 \ldots n_{el} \tag{7.2.3}$$

$$\mathbf{G}_e^* = \left(\delta_{\mathscr{S}_e} - \frac{l_e}{\Omega_e} \right) \mathscr{N}; \quad \mathscr{N} = \begin{bmatrix} n_x & 0 \\ 0 & n_y \\ n_y & n_x \end{bmatrix} \tag{7.2.4}$$

Substitution of Eq. (7.2.4) into Eq. (7.2.3) leads to:

$$\underbrace{\frac{1}{l_e} \int_{\mathscr{S}_e} \boldsymbol{\sigma}^h \cdot \mathscr{N} \, d\Gamma}_{\text{average on } \mathscr{S}_e} = \underbrace{\frac{1}{\Omega_e} \int_{\Omega_e \setminus \mathscr{S}_e} \boldsymbol{\sigma}^h \cdot \mathscr{N} \, d\Omega_e}_{\text{average on } \Omega_e \setminus \mathscr{S}_e} \tag{7.2.5}$$

Inspection of Eqs. (7.2.5) shows that they enforce Eq. (5.5) in average inside the element e. Therefore Eqs. (7.2.5) enforce, with mesh refinement, the traction vector continuity condition.

Remark 7.2.1 Use of the weak form (7.2.5) instead of the local form (5.5) allows to inscribe the proposed finite element approach in the framework of the assumed enhanced strain (A.E.S.) methods, Simo and Rifai (1990). The resulting discretized set of equations:

$$\int_{\Omega} \mathbf{B}^T : \boldsymbol{\sigma}^h \, d\Omega = \mathbf{f}_{ext}$$

$$\int_{\Omega_e} \mathbf{G}_e^{*T} \cdot \boldsymbol{\sigma}^h \, d\Omega_e = \mathbf{0} \quad e = 1 \ldots n_{el} \tag{7.2.6}$$

is sufficient for the determination of the set of unknowns $\mathbf{a}$ and $\boldsymbol{\alpha}_e$.

Remark 7.2.2 Observe that matrix $\mathbf{G}_e^*$ fulfills the following condition:

$$\int_{\Omega_e} \mathbf{G}_e^* \, d\Omega = 0 \tag{7.2.7}$$

as can be shown from Eq. (7.2.4). It is also possible to check, from inspection of Eqs. (7.1.5) and (7.1.6), that the spaces generated by the regular strains $\hat{\boldsymbol{\varepsilon}}^h$ and the enhanced strains $\tilde{\boldsymbol{\varepsilon}}^h$, denoted by $\hat{\mathscr{V}}^h$ and $\tilde{\mathscr{V}}^h$ respectively, are such that:

$$\hat{\mathscr{V}}^h \cap \tilde{\mathscr{V}}^h = \varnothing \tag{7.2.8}$$

Conditions (7.2.7) and (7.2.8) are sufficient to guarantee consistency and stability of the proposed assumed enhanced strain approximation, see Simo and Rifai (1990).

7.3 Regularization via delta-sequences. Regularized softening parameter. Integration rule

In the present approach we have to get round the obstacle of dealing with delta-functions, as the ones appearing in Eqs. (4.24), (7.1.6) and (7.2.4). In order to circumvent the difficulties inherent to perform computations involving Dirac's delta-functions in standard computers, we proceed to regularize the formulation by defining a delta-sequence, through a regularization parameter k, which converges to a delta-function when k tends to zero (in practice k can be as small as permitted by the machine precision). Therefore, the delta-function $\delta_{\mathscr{S}_e}$ is replaced by a regularized delta-sequence $\delta^k_{\mathscr{S}_e}$. The simplest way to construct $\delta^k_{\mathscr{S}_e}$ is by considering a finite band Ω^k_e of width k (see Fig. 7.a), from now on termed the elemental discontinuity band, around the elemental discontinuity line $\mathscr{S}_e$, and defining (see Fig. 7b):

$$\delta^k_{\mathscr{S}_e}(\mathbf{x}) = \begin{cases} \dfrac{1}{k} & \forall \mathbf{x} \in \Omega^k_e \\ 0 & \forall \mathbf{x} \in \Omega_e \setminus \Omega^k_e \end{cases} \tag{7.3.1}$$

In view of Eq. (7.3.1) the softening parameter $\mathscr{H}$ of Eq. (4.2.4) can be replaced in the constitutive equation by the regularized softening parameter $\mathscr{H}^k$ defined as:

$$\mathscr{H}^k(\mathbf{x}) = \begin{cases} k\bar{\mathscr{H}} & \forall \mathbf{x} \in \Omega^k_e \\ \infty & \forall \mathbf{x} \in \Omega_e \setminus \Omega^k_e \text{ (elastic behaviour)} \end{cases} \tag{7.3.2}$$

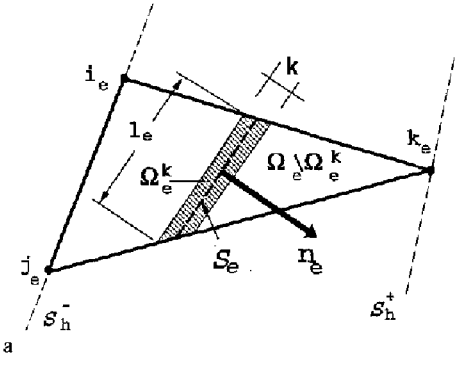

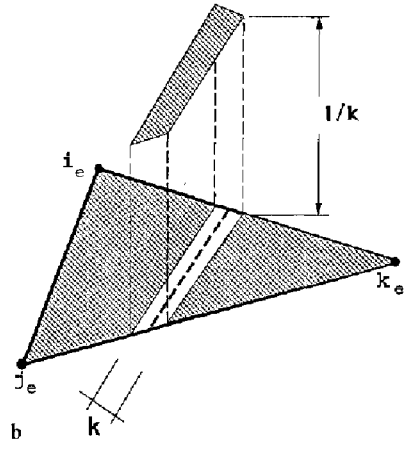

Fig. 7a–b. Regularized delta-sequence

Remark 7.3.1 To some extent the regularization parameter k plays, in the present formulation, the role of the so called characteristic length in some continuum models for capturing localization phenomena, Oliver (1989), which has a direct dependence on the mesh size. In both cases this parameter affects the slope of the softening branch of the constitutive equation but here k does not depend on the mesh size at all. Equation $(7.3.2)_1$ shows that, when k tends to zero, the limit case of perfect damage ($\mathscr{H} = 0$) is approached.

Consideration of the elemental discontinuity band Ω_e^k suggests an specific numerical integration rule for the described element. Inspection of the resulting formulation in previous sections, in view of Eqs. (7.3.1) and (7.3.2), reveals that the strains (and consequently the stresses) are constant in both the domain Ω_e^k and $\Omega_e \backslash \Omega_e^k$. Thus, after examining the set of equations to be solved (7.2.6) we conclude that only one integration point is needed in each of those domains, whose weight is the corresponding area as indicated in Fig. 8.

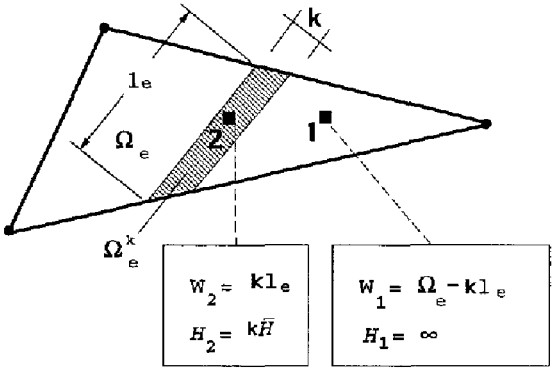

Fig. 8. Numerical integration rule and regularized hardening-softening parameter

8
Numerical simulations

8.1
Uniaxial plane-stress test

In Fig. 9 the considered geometry and boundary conditions are depicted. Under the assumed plane stress conditions the analytical solution of the problem can be obtained: perturbation of the peak stress σ_u at a certain material point leads to the formation of a strong discontinuity, along a straight line passing through the perturbed point. The inclination angle θ of the discontinuity line with respect to the x axis is given by:

$$\theta = \sqrt{\nu} \tag{8.1.1}$$

where ν stands for the Poisson's ratio. The analytical solution also exhibits an uniaxial and uniform stress field given by: $\sigma_x = \sigma$, $\sigma_y = 0$, $\tau_{xy} = 0$. In Fig. 10 numerical simulations for

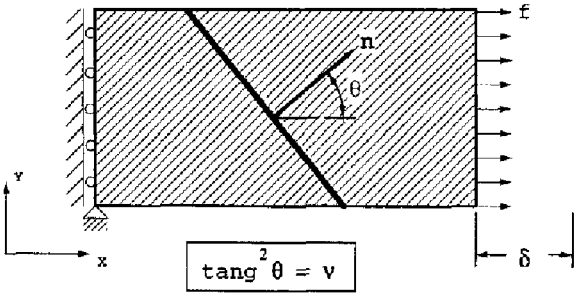

Fig. 9. Uniaxial tension test: definition of the problem

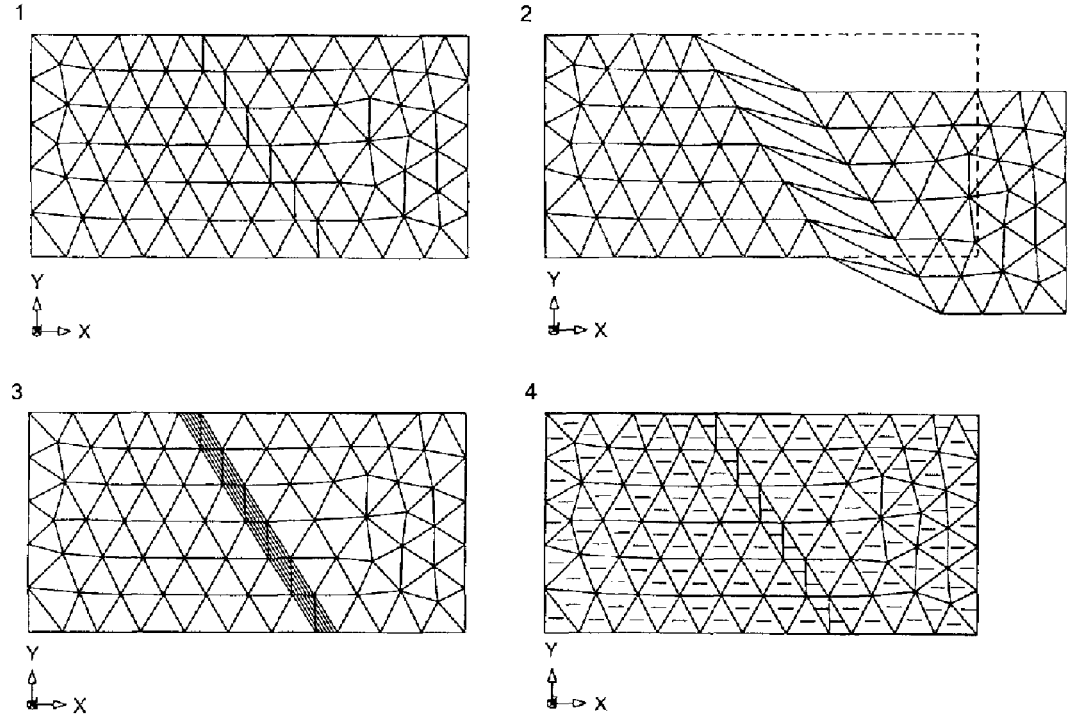

Fig. 10. Uniaxial tension test: results with the structured mesh

$\nu = 0.4$ are presented. Thus, from Eq. (8.1.1), a value of $\theta = 32.21°$ is expected for the inclination angle. In a first stage a finite element mesh with a structured band of elements defined by two parallel lines with this inclination is considered (see Fig. 10.1). The peak stress of the upper element of this band is slightly reduced (1%) in order to trigger the discontinuity. Fig. 10.2 shows the deformed mesh (amplified 100 times)[3] which corresponds to an almost rigid body motion of the frontal part of the specimen. Observe that the jump is perfectly captured by the inclined band as is stated in Fig. 10.3 by the contours of the total displacement field, which uniformly group inside this band. Fig. 10.4 shows the principal stress field which is uniaxial and perfectly uniform.

Results in Fig. 11 are force-displacement ($f - \delta$) curves at the end of the specimen for different values of the regularization parameter ($k = 1.0\text{e-}03$ and $k = 1.0\text{e-}09$) and the width the structured band ($h = 1.0$ and $h = 0.01$). In both cases the differences are indistinguishable in the plots, so complete insensitivity with respect to the value of the regularization parameter, assumed to be small enough with respect to the

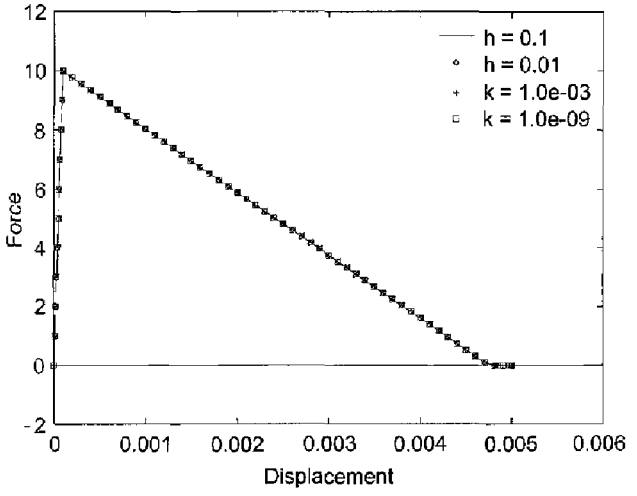

Fig. 11. Uniaxial tension test: Sensitivity analysis with respect to the regularization parameter, k, and the finite element size, h

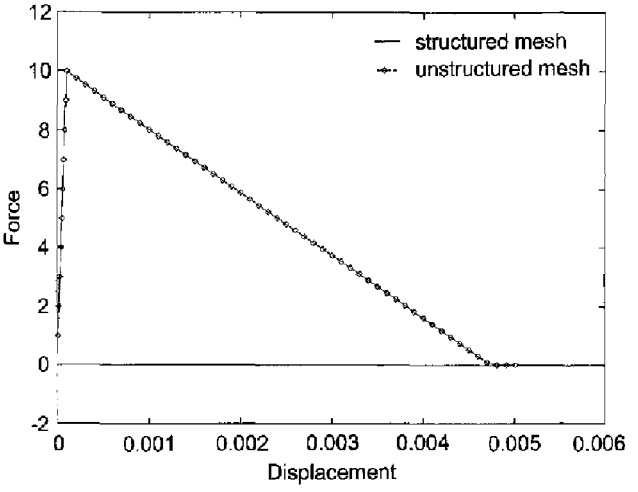

Fig. 13. Uniaxial tension test: force-displacement curves for the structured and the unstructured meshes

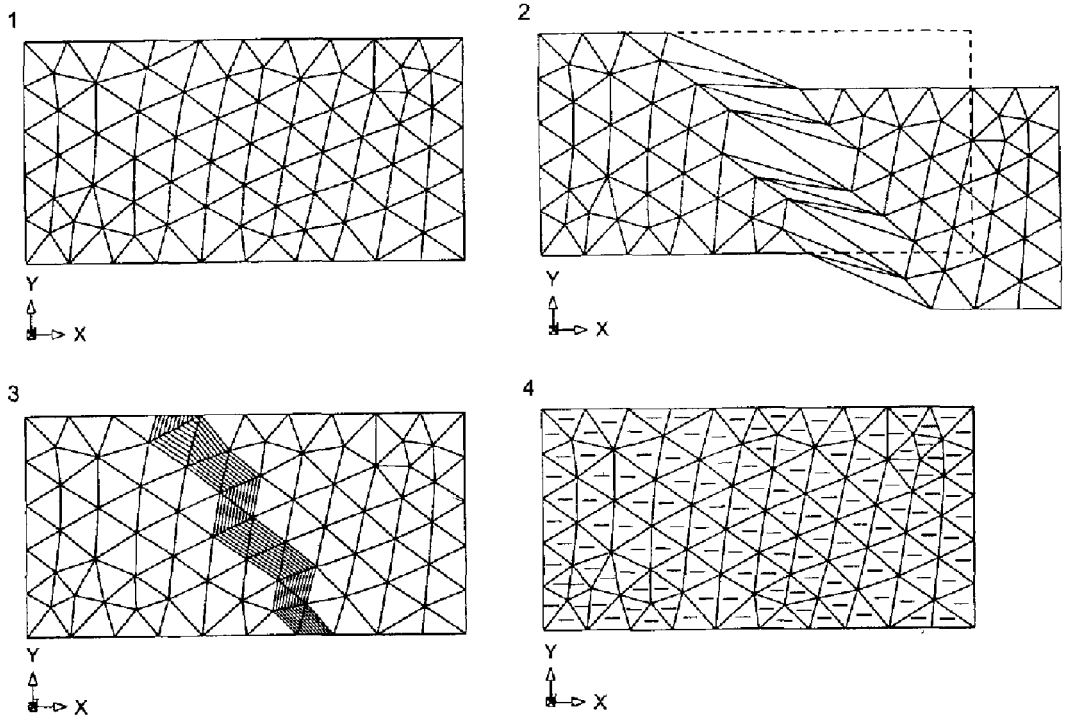

Fig. 12. Uniaxial tension test: results with the unstructured mesh

[3] For all the results presented here, postprocessing is based on the nodal values corresponding to the regular displacement field $\hat{\mathbf{u}}^h(\mathbf{x}, t)$ (see Eq. (7.1.1)). Thus, the enriching incompatible modes are not considered for postprocessing purposes

size of the element, and to the size of the finite elements capturing the jump (mesh size objectivity) is shown. In a second stage the same problem is analyzed with a completely unstructured finite element mesh (see Fig. 12.1). Again the

computed deformed mesh (Fig. 12.2), contours of the total displacement (Fig. 12.3) and the principal stress field (Fig. 12.4) are presented. The results are exactly the same than in the previous case. The only difference is that, now, the discontinuity is captured by a band of elements which zig-zagges through the mesh. It can be checked that it is possible to place a straight line inside this band with the expected inclination angle ($\theta = 32.31°$).

In Fig. 13 the force-displacement curves at the end of the specimen are compared for the structured and the unstructured mesh cases. Both curves are indistinguishable in the plot, thus, complete insensitivity with respect to the mesh alignment is exhibited.

8.2
Mode I fracture simulation

A more general test corresponds to a Mode I fracture simulation of the notched specimen depicted in Fig. 14.a, using the finite element mesh of Figure 14.b. The mesh is completely unstructured and refined around the zone where the discontinuity is expected to appear. Figure 15 shows the progression of the resulting crack for increasing times of the analysis. The discontinuity path can be identified by the contours of the displacement field, which group along the path of elements that capture the crack thus resulting in the dark paths of the figure. The crack initiates at the notch tip and then progresses verticaly as expected. Although the path of elements crossed by the discontinuity line zig-zagges vertically along the mesh, the discontinuity line (not plotted) is exactly a vertical line.

Figure 16 shows the deformed mesh (amplified 300 times) at the end of the analysis and a projection of the total displacement along the third dimension. Observe the symmetry of the deformed mesh (not imposed in the analysis since the mesh is unsymmetric), the strong localization of the apparent strain along the band of finite elements capturing the discontinuity and the linear variation of the apparent jump.

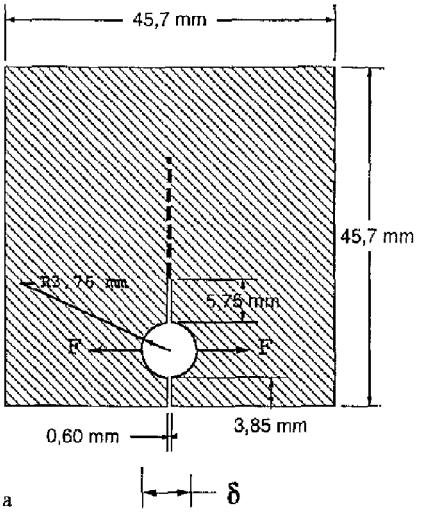

a

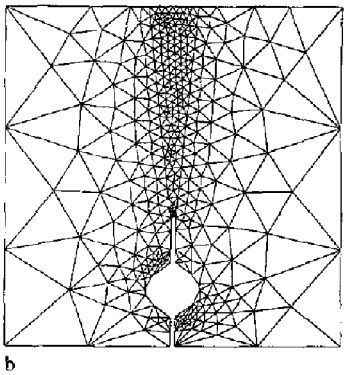

b

Fig. 14a–b. Mode I fracture simulation: a geometry and loading b finite element mesh

9
Concluding remarks

The main conclusion of the preceding work is that continuum approaches, based on standard (local, rate-independent, stress-strain) constitutive equations, can be recovered for the purposes of numerical simulation of strong discontinuities. Classical drawbacks inherent to such a type of approaches (mesh-size and mesh-alignment sensitivities) can be removed by making use of the following ingredients:

I) The strong discontinuity analysis. It provides the theoretical framework in which numerical simulations have to be settled. In particular the following key points can be extracted:

- The distributional character of the softening parameter
- The elastic (in general strain-hardening) behaviour outside the discontinuity surface.
- The strain-softening behaviour at the discontinuity interface. This provides a discrete constitutive equation, consistent with the continuum constitutive equation. Although this discrete equation can be explicitely derived and used in a discrete approach, see Armero and Garikipati (1995), there is no intrinsic necessity to perform such a derivation, and, as shown above, the actual analysis can be kept in a continuum framework by resorting to regularization procedures.
- The traction vector continuity condition, at the discontinuity surface, provides the jump.
- The stress field, at the initiation time, provides the value of the normal to the discontinuity surface.

II) *Specific finite element approaches.* Standard (continuous) finite elements have to be enriched to be able to capture discontinuities without resorting to local mesh refinement as, for instance in Zienkiewicz, Huang and Pastor (1995). In this work excellent results have been obtained, for 2D cases, by using incompatible discontinuous modes enriching the regular displacement field provided by standard linear triangles. A relevant feature of the presented finite element approach is that special alignments of the element sides (as in Larsson Runesson and Ottosen (1993)) are not required here. On the other hand the approach can be placed in the general framework of the assumed enhanced strain methods, thus enjoying all the advantages of these methods (in particular the easiness of implementation). Since the support of the incompatible modes is the element, they can be condensed at elemental level, thus, not contributing to enlarge the size of the

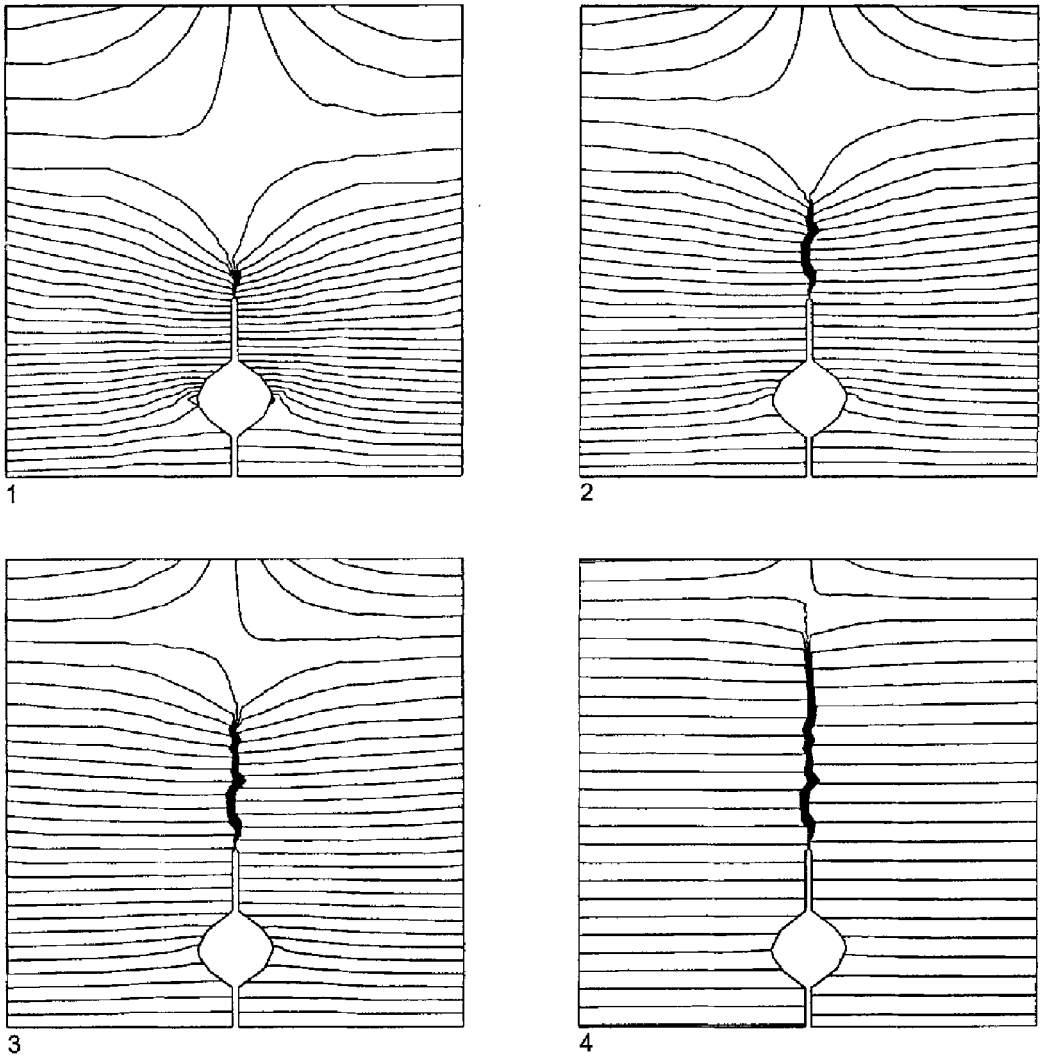

Fig. 15. Mode I fracture simulation: from 1) to 4) progression of the discontinuity path for increasing times of the analysis

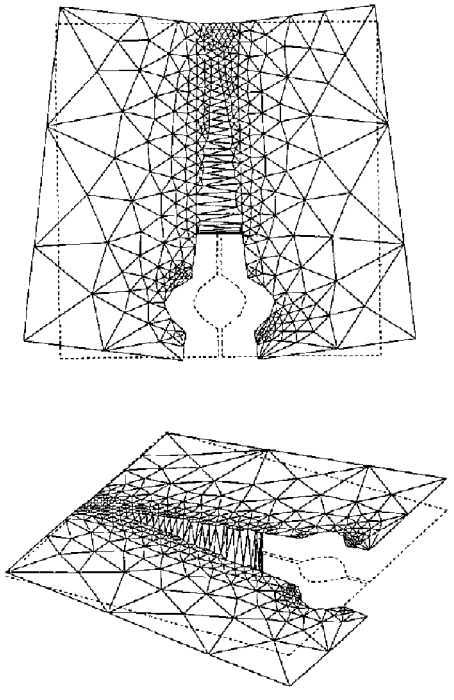

Fig. 16. Mode I fracture simulation: Up) deformed mesh (amplified 300 times) Down) 3D representation of the jump (the total displacement values are plotted along the third dimension)

nonlinear discretized system to be solved. The use of regularized delta-functions and regularization of the softening parameter has proved successful for a wide range of the regularization parameter values.

References

Armero F.; Garikipati K. 1995: Recent advances in the analysis and numerical simulation of strain localization in inelastic solids. In: D.R.J. Owen et. al. (ed): Proc. of the Fourth Conference on Computational Plasticity: Fundamentals and Applications, pp. 547–561, Swansea: Pineridge Press

Belytschko T.; Fish J.; Engelmann B. E. 1988: A finite element with embedded localization zones. Comp. Meth. Appl. Mech. Eng., 70: 59–89

De Borst R.; Muhlhaus H. B.; Pamin J.; Sluys L. J. 1992: Computational Modelling of Localisation of Deformation. In: D.R.J. Owen et al. (ed): Proc. of the Third Conference on Computational Plasticity: Fundamentals and Applications, pp. 483–508, Swansea: Pineridge Press

Dvorkin E. N.; Cuitiño A. M.; Gioia G. 1990: Finite elements with displacement interpolated embedded localization lines insensitive to mesh size and distortions. Int. Journ. Num. Meth. Eng., 30: 541–564

Larsson, R.; Runesson K.; Ottosen N. S. 1993: Discontinuous displacement approximation for capturing plastic localization. Int. Journ. Num. Meth. Eng., 36: 2087–2105

Lofti H. R.; Shing P. B. 1994: Analysis of concrete fracture with an embedded crack approach. In: H. Mang et. al. (ed): Proc. EURO-C 1994 Computer Modelling of concrete structures, pp. 343–352, Swansea: Pineridge Press

Needleman A. 1988: Material Rate Dependence and Mesh Sensitivity in Localization Problems. Comp. Meth. Appl. Mech. Engng., 67, 69–86

Oliver J. 1989: A consistent characteristic length for smeared cracking models. Int. Journ. Num. Meth. Engng., 28: 461–474

Oliver J.; Cervera M., Oller S., Lubliner J. 1990: Isotropic damage models and smeared crack analysis of concrete. In: N. Bicanic et. al. (ed): Proc. SCI-C Computer Aided Analysis and Design of Concrete Structures, pp. 945–957, Swansea: Pineridge Press

Oliver J.; Simo J. C. 1994: Modelling strong discontinuities by means of strain softening constitutive equations. In: H. Mang et. al. (ed): Proc. EURO-C 1994 Computer Modelling of concrete structures, pp. 363–372, Swansea: Pineridge Press

Pijaudier Cabo T. G.; Bazant Z. P. 1987: Nonlocal Damage Theory. Jour. Engng. Mesh., A. S. C. E., 113: 1512–1533

Simo, J. C.; Rifai, S. 1990: A class of mixed assumed strain methods and the method of incompatible modes. Int. Journ. Num. Meth. Engng., 29, 1595–1638

Simo J. C.; Oliver, J.; Armero F. 1993: An analysis of strong discontinuities induced by strain-softening in rate-independent inelastic solids. Computational Mechanics, 12: 277–296

Simo J. C.; Oliver, J. 1994: A new approach to the analysis and simulation of strong discontinuities. In: Z. P. Bazant et. al. (ed) Fracture and Damage in Quasibrittle Structures, pp. 25–39, E and FN Spon

Willam K.; Sobh N. 1987: Bifurcation analysis of tangential material operators. In: G. N. Pande et. al. (ed): Proc. NUMETA-87 Transient/Dynamic Analysis of Constitutive Laws for Engineering Materials, pp. C4/1-C4/13, Dordrecht: Martinus Nijhoff Publishers

Zienkiewicz O. C.; Taylor R. L. 1989: The Finite Element Method, London: McGraw-Hill

Zienkiewicz O. C.; Huang M.; Pastor M. 1995: Localization problems in plasticity using finite elements with adaptive remeshing. Int. Journ. Num. Meth. Eng., 19: 127–148